Neuronal differentiation and activity drive nucleocytoplasmic shuttling of the intellectual disability kinase TLK2

Lubna Nuhu-Soso, Heidi Denton, Darren L Goffin, Ines Hahn, Gareth J.O. Evans[#]

Department of Biology and York Institute of Biomedical Sciences, University of York, Wentworth Way, Heslington, York, YO10 5DD, United Kingdom

[#]Corresponding author: gareth.evans@york.ac.uk

Keywords
kinase, neurodevelopmental disorder, nuclear localisation signal, neuronal differentiation, splice variant

Abstract

Mental retardation autosomal dominant 57 (MRD57) is a rare neurodevelopmental disorder characterised by delayed language and psychomotor development, intellectual disability, hypotonia, gastrointestinal issues and facial dysmorphia. It is linked to genetic mutations in the serine/threonine kinase TLK2, characterised by haploinsufficiency and in some cases, its loss or impaired kinase function. TLK2 is an established cell cycle regulator that has been extensively studied in mitotic cells. It is upregulated in cancers, driving tumour growth, however, the role of TLK2 in postmitotic neurons is not understood. We therefore aimed to gain insight into how TLK2 mutations cause MRD57 by determining where TLK2 is expressed in the brain and its subcellular localisation during neuronal differentiation. Public human and mouse brain transcriptomic data revealed splice variant diversity in the N-terminus of TLK2, which contains its nuclear localisation sequence (NLS). Using splice-specific *in situ* hybridisation probes, we observed expression of TLK2 isoforms that contain and lack the NLS in the mouse hippocampus and cerebellum. We confirmed these findings in human SH-SY5Y neuroblastoma cells, and found that neuronal differentiation of these cells enhances a cytoplasmic pool of TLK2 by two mechanisms: nuclear export of full length TLK2 and increased expression of TLK2 splice variants lacking the NLS. Finally, acute stimuli that mimic synaptic activity were sufficient to elicit nuclear export of TLK2. Our data highlight the need to establish the neuronal cytoplasmic substrates of TLK2 and determine how the loss of TLK2 activity in MRD57 might impact their function in the developing and mature brain.

Introduction

Tousled-like kinase 1 and 2 are the mammalian homologues of the *Arabidopsis* mutant, *tousled*, which was discovered in a developmental screen (Roe et al., 1993). Indeed, both human TLK1 and TLK2 have been linked with rare developmental disorders (Segura-Bayona and Stracker, 2019; Villamor-Payà et al., 2024). To date, there have been close to 50 documented patients worldwide with TLK2 mutations, classified as autosomal dominant Mental Retardation Disorder 57 (MRD57; (Lelieveld et al., 2016; Reijnders et al., 2018; Töpf et al., 2020; Pavinato et al., 2022; Woods et al., 2022), with a predicted incidence of approximately 3 in 100,000 individuals (López-Rivera et al., 2020). The clinical phenotypes associated with MRD57, like other neurodevelopmental disorders, are heterogeneous, including intellectual disability, delayed psychomotor development in infancy or early childhood, language delay, hypotonia, feeding problems, gastrointestinal issues, dysmorphic facial features, microcephaly, behaviour problems and global developmental delays (Reijnders et al., 2018; Töpf et al., 2020; Pavinato et al., 2022; Woods et al., 2022). The majority of TLK2 mutations in MRD57 are *de novo* mutations, but seven are inherited within four different families (Reijnders et al., 2018; Töpf et al., 2020; Pavinato et al., 2022). Like the *de novo* cases, inherited TLK2 mutations are heterozygous dominant except one report of a homozygous recessive inheritance (Reijnders et al., 2018; Töpf et al., 2020; Pavinato et al., 2022). MRD57 patients have TLK2 mutations throughout the protein and all are predicted to result in a reduction of TLK2 expression or its catalytic activity (Mortuza etc).

Functionally, TLK2 is an established regulator of DNA replication, cell cycle checkpoint recovery and chromatin remodelling (Bruinsma et al., 2016; Kim et al., 2016a; Segura-Bayona et al., 2017; Silljé et al., 1999). TLK2 facilitates cell cycle progression mainly by enhancing histone supply via phosphorylation of its best characterised substrate, ASF1 (Klimovskaia et al., 2014). In-line with other cell cycle kinases, TLK activity and gene copy number are increased in cancer, including breast, cervix, lung, liver, colon and kidney (Bhoir and De Benedetti, 2023; Kim et al., 2016b; Lee et al., 2018). The chromosomal locus of TLK2, 17q23, contains other oncogenes, and is frequently amplified in more than 40% of breast cancer tumours (Kelemen et al., 2009; Kim et al., 2016b). Moreover, single nucleotide polymorphisms (SNPs) in TLK2 have been identified as risk factors for breast cancer (Kelemen et al., 2009). Indeed, inhibition of TLK2 has been identified as a therapeutic strategy and small molecule inhibitors are in development (Kim et al., 2016b; Lee et al., 2018).

In contrast to its role in the cell cycle and cancer, the neuronal expression and cell biology of TLK2 is poorly understood. Here we have characterised its neuronal transcript expression, revealing a conserved splice diversity in rodents and humans. TLK2 alternative splicing occurs in exons encoding the N-terminus, resulting in ‘long’ and ‘short’ isoforms, with the latter lacking the nuclear localisation sequence (NLS). Expression of both long and short TLK2 isoforms is prevalent in neurons of the mouse hippocampus and cerebellum. Using a cell model of neuronal differentiation, we observed the upregulation of short TLK2 expression during neuronal differentiation, with a concomitant shuttling of long TLK from the nucleus to the cytoplasm. Pharmacological treatments mimicking neuronal activity also drive nucleocytoplasmic shuttling of TLK2. These data highlight the likely importance of cytoplasmic TLK2 in terminally differentiated neurons, which have exited the cell cycle. There

is hence a need to determine the neuronal substrates of TLK2 to shed light on the neuronal phenotypes of MRD57.

Materials and Methods

Materials

SH-SY5Y and Flp-In T-REx SK-N-SH neuroblastoma cell lines were kind gifts from Dr Andrew Stoker, University College London and Dr Han-Jou Chen, University of York respectively. The Flp recombinase expression vector, pOG44 was a kind gift from Dr Paul Pryor, University of York.

Bioinformatics

TLK2 transcript IDs and exon structures were derived from their Ensembl gene annotations (version 113) using human (GRCh38.p14) or mouse (GRCm39) genome builds (Harrison et al., 2024). The human TLK2 RNAseq data used for the transcriptomic analyses described in this manuscript were obtained from the GTEx Portal, accession number phs000424.v8.p2. Mouse brain TLK2 RNAseq data was obtained from the Human Protein Atlas (proteinatlas.org; (Sjöstedt et al., 2020)). TLK2 transcript expression values in transcripts per million (TPM) were converted to percentages by tissue or brain region.

RNA extraction, cDNA synthesis and RT PCR

All work involving mice was approved by the University of York Animal Welfare and Ethical Review Body and performed under UK Home Office legislation (project licence P38B2013E). Adult wild-type C57BL/6 mouse forebrain and cerebellum were dissected and homogenised in RIPA buffer (50 mM Tris, pH 8.0, 150 mM NaCl, 1% (v/v) Triton-X-100, 0.5% (w/v) sodium deoxycholate, 0.1% (w/v) SDS, 1 mM EDTA supplemented with 1 mM Na_3VO_4, 0.1% (v/v) β-mercaptoethanol, 1 mM PMSF and 1:200 protease inhibitor cocktail (Sigma)) using 5 ml buffer/g of tissue. The homogenate was incubated at 4°C with agitation for 1 h and then centrifuged at 20,000*g* for 30 min at 4°C. RNA was extracted from the supernatant. SH-SY5Y cells undergoing neuronal differentiation were plated at 10^4 cells/ cm^2 onto collagen coated 6-well tissue culture dishes. RNA was extracted from the differentiating cells at two day intervals. For both mouse brain and SH-SY5Ys, RNA was extracted using a NucleoSpin RNA isolation kit (Macherey-Nagel) according to the manufacturer's instructions. Complementary DNA was synthesised from 1 µg of RNA using a SuperScript IV First-Strand cDNA Synthesis Kit (Life Technologies) according to the manufacturer's instructions in the presence of both oligo $d(T)_{18}$ and random hexamer primers. A no RT cDNA sample was performed for each time point and cDNA was stored at -20°C. PCR reactions were performed in 25 µl reactions containing 1 µl of cDNA, 1X GoTaq flexi buffer, 0.2 mM each of dNTP mix, 0.4 µM of each primer pair (Table 1) and 1U Taq polymerase. Cycling conditions consisted of an initial denaturing step at 98°C for 30s followed by 25-30 cycles of 95°C for 10s, 55°C for 30s, 72°C for 1 min/kb and a final extension at 68°C for 10 min. 5 - 10 µl of the PCR products were separated on 1.5-2% (w/v) agarose gels to confirm amplification.

In situ hybridisation

Mice were anaesthetised with isoflurane inhalation followed by an intraperitoneal injection of 100 mg/kg ketamine and 12.5 mg/kg xylazine and then transcardially perfused with 4% paraformaldehyde (PFA) in 0.1 M sodium-potassium PBS. The brain dissected and post-fixed in 4% PFA overnight at 4°C. Following a further 24 h incubation in 30% sucrose, brains

were embedded in OCT, frozen at -80°C, and 25 µm coronal or sagittal sections were cut using a Leica CM1950 cryostat. Probes for *in situ* hybridisation were transcribed using 10X digoxigenin (DIG) RNA labelling mix (Roche) and T7 polymerase. For *in vitro* transcription, template DNA was synthesised as gBlocks™ (IDT) and PCR amplified to introduce the T7 promoter sequence (Table 1). *In situ* hybridisation was performed according to (Fisher et al., 2002) with adaptations for sections mounted on slides. Briefly, the sections were first incubated in 4% PFA for 10 min at room temperature (RT) followed by two 5 min PBST washes. Sections were then treated with 4 µg/ml proteinase K (Roche) in PBST for 10 min and then washed twice in PBST for 5 min. A second fix in 4% (w/v) PFA was performed for 10 min, followed by two 5 min PBST washes. Next, the sections were acetylated using 0.5% (v/v) acetic anhydride in 0.1 M triethanolamine, pH 7.8 for 10 min followed by two 5 min PBST washes and finally a 15 min wash in 5X saline-sodium citrate buffer (SSC; Sigma). Pre-hybridisation was carried out by incubating the sections in hybridisation buffer (50% (v/v) formamide (Ambion, AM9342), 5X SSC, 100 µg/ml heparin, 1X Denhardt's, 0.1% (v/v) Tween-20, 0.1% (w/v) CHAPS, 10 mM EDTA, 1 mg/ml total yeast RNA) containing no probe at 65°C for 2-5 h in a humidified box. Hybridisation followed by incubating the sections with 300 ng/ml of probe solution (DIG prep in hybridisation buffer) overnight at 65°C in a humidified box.

Post-hybridisation, the sections were subjected to several hot wash steps. First a 10 min wash in hybridisation buffer containing no probe at 65°C, then a 1 h wash in 2X SSC followed by a 1 h wash in 0.2X SSC, both at 65°C. The sections were then washed twice for 5 min in MABT (100 mM maleic acid, 150 mM NaCl, 0.1% (v/v) Tween-20, pH 7.8) at RT and then blocked in blocking solution (2% (w/v) Boehringer Mannheim Blocking Reagent (Roche, 11096176001), 20% (v/v) heat-treated lamb serum (Sigma), 1X MAB) for 2 h at RT in a humidified box. Next, the sections were incubated with anti-DIG-AP (Table 2) in blocking solution overnight at 4°C in a humidified box. Post-antibody washes were carried out at RT by washing the sections three times for 1 h in MABT and once in alkaline phosphatase (AP) buffer (100 mM Tris, pH 9.5, 50 mM $MgCl_2$, 100 mM NaCl) for 10 min. The colour reaction was initiated by adding a 1:3 dilution of BM purple (Roche, 11442074001) in AP buffer to the sections and incubation at RT in a humidified box for 1-5 days. The reaction was stopped by washing the sections twice for 10 min in PBST, fixing in 4% (w/v) PFA for 1 h or overnight at 4°C and a 15 min wash in PBST. The sections were air dried, mounted in aqueous mounting media (Sigma, 324590) and stored at 4°C. Images were acquired on a Leica DM2500 microscope with a 10X objective (sagittal) and a Zeiss Stemi 508 stereo microscope (coronal).

Table 1. Primers and probes used in this study

Name	Sequence (5'-3')
PCR primers	
mTLK2-exon1 sense	GACCCACGAAGGCAGGAATTA
mTLK2-exon5/6 anti	CTCGACGCGGTAAGGGATTG
mTLK2-exon4/6 anti	CTGCTCGACGCTCAAAGTAA
mTLK2-exon3/6 anti	GCTCGACGCTTGGCTAGT
mTLK2-exon6 anti	GCTGCACTGCCATCTAAACC
mGAPDH sense	CATCACTGCCACCCAGAAGACTG
mGAPDH anti	ATGCCAGTGAGCTTCCCGTTCAG
hTLK2-exon1 sense	ATTGCATAGCCTGGACCCAC

hTLK2-exon9 anti	TCGTTCCTTGTATTTCTCTAGCA
hMAPT sense	ACACCATGCACCAAGACCAA
hMAPT anti	TCCTTCTGGGATCTCCGTGT
hGAPDH sense	GTCTCCTCTGACTTCAACAGCG
hGAPDH anti	ACCACCCTGTTGCTGTAGCC
ISH probes	
mTLK2-204	GGAACCAGCCCTGGCAGAAGTGTTCCACCAGTTGCACGATCCTCACCGCA ACATTCCTTATCCAATCCCTTACCGCGTCGAGCAGAACAGCCTCTGTATG GTTTAGATGGCAGTGCAGCAAAGGAGGCCTCAGAAGAGCAGTCTGCTCTG
mTLK2-201	AGGAAAGCCGAGCCATATGACACTAGCCAAGGGAAAGGCACTCCTAGGGG ACATAAAATTAGTGATTACTTTGAGCGTCGAGCAGAACAGCCTCTGTATG GTTTAGATGGCAGTGCAGCAAAGGAGGCCTCAGAAGAGCAGTCTGCTCTG
mTLK2-207	TAGAGACTCCTGAGAAAAAGCAGAATGACCAGCGAAATCGGAAAAGGAAA GCCGAGCCATATGACACTAGCCAAGCGTCGAGCAGAACAGCCTCTGTATG GTTTAGATGGCAGTGCAGCAAAGGAGGCCTCAGAAGAGCAGTCTGCTCTG
mTLK2-novel	CAACCAGAGTCTGTGCAGCGTGGGGTCGTTGAGTGATAAAGAAGTAGAGA CTCCTGAGAAAAAGCAGAATGACCGCGTCGAGCAGAACAGCCTCTGTATG GTTTAGATGGCAGTGCAGCAAAGGAGGCCTCAGAAGAGCAGTCTGCTCTG
mCalb1	GATGCTTTGCTGAAAGATCTGTGTGAGAAGAACAAACAGGAATTGGATAT TAACAATATTACTACATACAAGAAGAACATAATGGCCTTGTCGGATGGAG GGAAGCTGTACCGAACAGACCTTGCTCTTATTCTTTCTGCTGGAGACAAC

Culture, neuronal differentiation and pharmacological treatment of SH-SY5Y cells

SH-SY5Y cells were maintained at 37°C, 5% CO_2 in a humidified atmosphere in Dulbecco's Modified Eagle Medium (DMEM) with high glucose, pyruvate and L-glutamine supplemented with 10% foetal bovine serum (FBS) and 1% penicillin/streptomycin.

Neuronal differentiation of SH-SY5Y cells was performed according to a previously described method (Encinas et al., 2000). Briefly, tissue culture dishes or coverslips were coated in 0.05 mg/ml collagen in 60% (v/v) ethanol. Cells were plated at 10^4 cells/cm^2 (for protein analysis) or 5 x 10^3 cells/well (for microscopy) in DMEM supplemented with 15% (v/v) heat inactivated FBS and 1% (v/v) penicillin/streptomycin. Twenty four hours after plating, the media was changed and supplemented with 10 µM retinoic acid (RA; Sigma, R2625). Six days after plating, the cells were washed three times in serum-free DMEM and then incubated with serum-free DMEM containing 50 ng/ml brain-derived neurotrophic factor (BDNF; Qkine) and 1% (v/v) penicillin/streptomycin and cultured for a further seven days. Throughout the differentiation process, the media was changed every two days and supplemented with the appropriate differentiation agent.

For analysing protein expression in differentiating cells, lysates were collected at two day intervals. Cells were washed twice in sterile ice-cold PBS and scraped in 100 µl of lysis buffer (20 mM HEPES, pH 7.4, 10 mM KCl, 2 mM $MgCl_2$, 1 mM EDTA and 1 mM EGTA, 1 mM DTT and protease inhibitor cocktail). Lysates were incubated on ice for 15 min, passed through a 25G needle ten times and protein concentration was determined by Bradford assay. The lysates were diluted in Laemmli sample buffer, boiled for 10 min at 90°C and 10 µg of protein was separated by SDS-PAGE and analysed by Western blotting.

Pharmacological stimulation of undifferentiated SH-SY5Y cells was performed on cells plated 24 h prior to treatment on 13 mm coverslips in a 24-well plate at 5 x 10^4 cells/well. Cells were washed twice in PBS and then incubated for 1 h at 37°C, 5% CO_2 in either control buffer (170 mM NaCl, 3.5 mM KCl, 0.4 mM KH_2PO4, 10 mM HEPES, 5 mM $NaHCO_3$, 5 mM glucose, 1.2 mM Na_2SO_4, 1.2 mM $MgCl_2$, 1.3 mM $CaCl_2$, pH 7.4, 0.2% (v/v) DMSO) or KCl/FSK buffer

181 (control buffer with 73.5 mM NaCl, 100 mM KCl, 10 μM forskolin, 100 μM IBMX, 0.2% (v/v)
182 DMSO). Cells were then fixed and immunocytochemistry was performed as described below
183 using anti-TLK2.
184
185 **Inducible stable TLK2 cell lines**
186 Tetracycline-inducible SK-N-SH cell lines expressing either full length TLK2-203 or short N-
187 terminally truncated TLK2-213 were generated using the Flp-In™ T-REx™ System
188 (Invitrogen). pcDNA5/FRT/TO-FLAG-TLK2 was purchased from the MRC PPU Reagents
189 and Services facility (College of Life Sciences, University of Dundee). TLK2-213 was made
190 by subcloning its ORF from full length TLK2 and ligating it back into the same backbone via
191 5' and 3' NotI restriction sites with the N-terminal FLAG tag intact. Cells were co-transfected
192 with the FRT backbone containing the gene of interest (TLK2-203 or TLK2-213) and a Flp-
193 recombinase expression vector (pOG44). Positive clones were selected by treating with 0.5
194 mg/ml hygromycin B and assaying for protein expression after the addition of 1 μg/ml
195 doxycycline.
196
197 **Subcellular fractionation**
198 Flp-In SK-N-SH cells were fractionated according to the Abcam subcellular fractionation
199 protocol. TLK2 expression was induced using 1 μg/ml doxycycline and left in culture for 48 h
200 prior to fractionation. Briefly, cells were scraped in 500 μl of lysis buffer (described above)
201 and incubated on ice for 15 min. The scraped cells were passed through a 25G needle ten
202 times, incubated on ice for 20 min and then centrifuged at 720*g* for 5 min at 4°C. The post-
203 nuclear supernatant was transferred to a fresh tube. The nuclear pellet was washed by first
204 resuspending in lysis buffer, passing the sample through a 25G needle ten times and
205 centrifuging at 720*g* for 10 min at 4°C. The washed pellet was resuspended in TBS
206 containing 0.1% (w/v) SDS, and sonicated on ice for 3 s. The protein concentration of each
207 fraction was determined by Bradford assay and 20 μg of each fraction was separated by
208 SDS-PAGE and analysed by Western blotting.
209
210 **Western blotting**
211 Proteins separated by SDS-PAGE (7.5-12%) gels were transferred onto PVDF membranes
212 (Millipore). Membranes were incubated with primary antibodies (Table 2) overnight at 4°C
213 with agitation. Membranes were washed and incubated with appropriate HRP-conjugated
214 secondary antibodies and immunoreactivity was visualised by incubation with enhanced
215 chemiluminescence reagent and imaged on an iBright FL1000 scanner (Invitrogen).
216
217 **Immunocytochemistry and fluorescence microscopy**
218 Cells were washed 3x in PBS and then fixed in 4% (w/v) paraformaldehyde (PFA) in PBS for
219 20 min at RT. Next cells were washed 3x in PBS then permeabilised and blocked in PBS
220 containing 0.1% (v/v) TritonX-100 and 1% (w/v) bovine serum albumin (BSA). Primary
221 antibodies were diluted in PBS containing 1% (w/v) BSA at appropriate dilutions (Table 2)
222 and incubated on cells overnight at 4°C. Cells were washed 3x in PBS then incubated with
223 secondary antibodies in PBS containing 1% (w/v) BSA for 1 h in the dark at RT. Finally, cells
224 were washed 3x in PBS, 1x in dH_2O, air dried and mounted in Mowial containing 1 μg/ml
225 4′,6-diamidino-2-phenylindole (DAPI). Images were acquired in the Bioscience Technology
226 Facility (University of York) on a Zeiss LSM 880 confocal microscope on a 40x/1.4 Oil DIC III
227 objective.
228

229 **Table 2. Antibodies used in this study.**

Name	Dilution	Species	Catalogue no.	Supplier
Primary antibodies				
Anti-TLK2	1:1000 (WB) 1:500 (IF)	Rabbit	A301-257A	Bethyl
Anti-β-III-tubulin	1:1000 (WB) 1:500 (IF)	Mouse	801202	Biolegend
Anti-β-actin	1:50000 - 1:100000	Mouse	60008-1-Ig	Proteintech
Anti-Histone H3	1:5000	Mouse	819411	Biolegend
Anti-GAPDH	1:5000	Mouse	MAB374	Sigma
Anti-FLAG	1:1000	Mouse	F1804	Sigma
Anti-Digoxigenin	1:2000	Sheep	11093274910	Roche
Secondary antibodies				
Anti-mouse HRP	1:5000	Goat	A4416	Sigma
Anti-rabbit HRP	1:5000	Goat	A6154	Sigma
Anti-mouse Alexa 594	1:500	Goat	A11020	Invitrogen
Anti-rabbit Alexa 488	1:500	Goat	A11008	Invitrogen

230

231 **Data analysis**

232 Quantification of hippocampal *in situ* hybridization images was performed on 16 bit grayscale
233 images in FIJI (Schindelin et al., 2012). The oval selection tool was used to draw regions of
234 interest (ROI) in different locations within the hippocampal formation (CA1, CA3, DGs and
235 DGi). The intensity was then measured and normalised to DGs for each section and probe.
236 Three to four hippocampi were quantified for each probe and the values were plotted as a
237 heatmap in Morpheus (https://software.broadinstitute.org/morpheus).
238 The quantification of cytoplasmic/nuclear TLK2 ratios of immunofluorescent images was
239 conducted by measuring the TLK2 intensity in the nucleus and cytoplasm of the cells in FIJI
240 using the ROI 1-click plug-in (Thomas and Gehrig 2020). Three hundred cells for each
241 condition were analysed from three technical replicates (100 cells/replicate). Western blots
242 were quantified by densitometry analysis in FIJI. Statistical significance was assessed by t-

test or non-parametric ANOVA with Dunn's post-hoc test. Statistical analyses and graph plotting was performed in RStudio (RStudio Team, 2020).

Results

TLK2 is alternatively spliced in human and mouse brain

Since the neuronal distribution and function of TLK2 has not been investigated, we first sought to characterise TLK2 transcript expression in the brain. Previous studies have observed tissue-specific transcripts of TLK2, in the mouse testis for example (Shalom and Don, 1999), and TLK2 immunoblots often have multiple bands that vary between tissues and cell lines (Kim et al., 2016b; Segura-Bayona et al., 2017). Such bands could result from post-translational modifications or alternative splicing of TLK2 or a combination. We began by interrogating publicly available human (GTEx) and mouse brain (Human Protein Atlas) transcriptomic data to characterise neuronal TLK2 transcript expression (Figure 1A,B), focussing on the hippocampus and cerebellum. In the mouse brain, a full length transcript corresponding to the canonical Ensembl TLK2 transcript was the most abundant transcript (mTLK2-204; mouse TLK2 transcripts will be referred to here as 'mTLK2'). In the human brain, surprisingly the most abundant transcript was not canonical TLK2 (TLK2-203), but a transcript lacking exon 5 (TLK2-202; Figs. 1B, S1 & S2). We also identified further evolutionarily conserved splice variant diversity at the N-terminus of the protein, encoded by exons 1-9. Not surprisingly, there were fewer alternative splicing events in exons encoding the middle coiled-coil domain and C-terminal kinase domain of TLK2, which are essential for dimerisation and catalytic activity respectively (Mortuza et al., 2018); Figure 1B). Interestingly, splice variants lacking exon 3 in which the nuclear localisation sequence (NLS, Figure 1A) is located (Yamakawa et al., 1997) are also abundant (Figure 1B,S1). This suggests that a pool of TLK2 is constitutively resident outside the nucleus. Henceforth in this study we shall refer to isoforms that include the NLS as 'long TLK2', and those lacking the NLS as 'short TLK2'. In the human GTEx dataset it was observed that transcript TLK2-207 represents nearly a third of TLK2 mRNA expression, but is predicted to be subject to nonsense mediated decay due to an intron retention at exon 21 (Figure 1B).

To confirm the existence of alternative N-terminal TLK2 splice variants in the brain, we performed RT-PCR of mouse brain TLK2 mRNA. The annotated transcripts of mouse TLK2 have splice diversity within exons 1-6 (Figure 2A and Figure S2). We first amplified and sequenced all N-terminal splice variants in mouse forebrain or cerebellar cDNA using transcript-specific primers and also a pair of 'pan isoform' primers located in exon 1 (forward) and exon 6 (reverse), which yielded four bands (Figure 2A). Three of the bands corresponded to the 5' of annotated isoforms, two of which are predicted to contain the NLS (mTLK2-204 and -201) and one that lacks the NLS due to an alternative start site in exon 6 (mTLK2-207). We also sequenced a novel isoform that has a truncated exon 3, lacks exon 4 and 5 and would also not encode the NLS (mTLK2-novel; Figure 2B and Figure S2). We next used *in situ* hybridisation to observe whether there is any cell type specificity in the expression of these TLK2 isoforms in the brain. All mouse TLK2 transcripts express exon 6 and combinations of exons 1-5, therefore we designed a suite of short 150 bp splice junction-spanning *in situ* probes anchored at the 3' end by the first 75 bp complementary to exon 6 and containing a variable 5' 75 bp complementary to exons 5, 4 or 3 (Figure 2B).

290 In coronal and sagittal mouse brain sections we examined the expression of TLK2 isoforms in
291 the hippocampal formation and cerebellar cortex respectively. A 150 bp exon junction spanning
292 calbindin probe was used as a positive control, confirming calbindin expression in the Purkinje
293 neurons of the cerebellar cortex and dentate gyrus and CA1 neurons of the hippocampus
294 (Figure 2C,E). Low background staining was observed in the absence of an *in situ* probe
295 (Figure 2C,E). In the coronal sections, hippocampal staining of all TLK2 isoform probes was
296 detected in excitatory neurons of the dentate gyrus, CA1 and CA3 (Figure 2C). Although
297 quantifying the intensity of staining between probes was not appropriate, using regions of
298 interest placed in the DG, CA1 and CA3 fields, we quantified the relative intensity of staining
299 of each TLK2 isoform in these hippocampal cell types and normalised the density to the signal
300 in the suprapyramidal blade of the dentate gyrus (DGs; Figure 2C). The full length TLK2 (exons
301 1-6) probe, corresponding to the most abundant splice variant mTLK2-204, gave strong
302 staining in the cell soma of the granule neurons in the DG and pyramidal neurons in CA1 and
303 to a lesser extent in CA3 (Fig 2B, C). The other long TLK2 isoform (mTLK2-201) was less
304 readily detected in the hippocampus, but quantification revealed differential expression in the
305 two pyramidal blades of the DG, with the suprapyramidal blade having the highest intensity
306 (Figure 2D). The relative staining of the shorter variant, mTLK2-207, was highest in CA1
307 neurons. In-line with the PCR (Figure 2A), staining of the novel short TLK2 isoform appeared
308 weakest, with the highest intensity in CA1 and CA3 compared to the DG (Figure 2C, D).
309
310 In sagittal sections of the cerebellar cortex, staining of the TLK2 probes was readily detectable
311 in the abundant granule neurons and to a lesser extent in Purkinje neurons (Figure 2E). The
312 intensity of staining for the full length mTLK2-204 probe was similar to that of the shorter
313 mTLK2-207 in the granule cell and Purkinje layers, whereas the mTLK2-201 and mTLK2-novel
314 probes had weak granule layer staining and barely detectable staining of Purkinje neurons
315 (Figure 2E). For all TLK2 probes, we failed to observe staining of inhibitory interneurons in the
316 hippocampus or cerebellar cortex. Taken together, these data confirm the RNAseq data that
317 alternative splice variants of TLK2 are expressed in neurons of the mammalian brain. It is
318 currently unclear as to the physiological relevance of the neuronal cell-type specific expression
319 of these TLK2 variants we have observed.
320
321 **Alternative splicing of TLK2 is regulated during neuronal differentiation**
322 To date, our knowledge of TLK2 is mainly limited to its nuclear functions (Segura-Bayona and
323 Stracker, 2019). The possibility of a non-nuclear pool of TLK2 in post-mitotic neurons has
324 interesting implications for the role of TLK2 in the developing and mature brain. To study TLK2
325 expression in neuronal differentiation we adopted a protocol for differentiating the human
326 neuroblastoma cell line SH-SY5Y. Based on a previously published method we used the
327 sequential application of retinoic acid (RA) and then BDNF with serum withdrawal over several
328 days (Encinas et al., 2000), which produced robust neuronal morphology (Figure 3A) and
329 enhanced transcript expression of the neuronal marker tau (Figure 3B). To capture the diversity
330 of 5' TLK2 splice variants we performed RT-PCR on SH-SY5Y cDNA samples from day 1-13
331 with primers located in exons 1 (forward) and 9 (reverse). This yielded six bands (Figure 3B),
332 which were sequenced (Figure S3). Figure 3B summarises the exon structure of each TLK2
333 PCR product, any corresponding annotated Ensembl transcripts and the predicted mass of the
334 protein they encode. The three longest PCR products mapped onto several Ensembl
335 transcripts with alternative splicing of combinations of exons 5, 7 and 8. The top two bands
336 each potentially correspond to two Ensmbl isoforms due to alternative splicing at exon 12,
337 which wasn't amplified in the PCR reaction. These bands were also the most prominent PCR

338 products in HEK293 cells. Sequencing the third band yielded a mix of sequences that we were
339 unable to deconvolve, but likely comprises up to three isoforms of the same mass (Figure 3B,
340 S3). We were not able to detect expression of a transcript corresponding to TLK2-213, the
341 annotated TLK2 transcript that lacks the NLS (Figure 1B). Instead, the three smallest PCR
342 products represented novel isoforms lacking exons 3, 4 and 5, with alternative splicing of exons
343 2, 7 and 8 (Figure 3B). All three of these transcripts are predicted to be protein coding and lack
344 the NLS. HEK293 cells possessed very low levels of these PCR products.
345
346 We observed a striking regulation of TLK2 isoform expression during neuronal differentiation
347 of the SH-SY5Y cells (Figure 3B). In undifferentiated cells the TLK2 isoforms are dominated
348 by the long transcripts (TLK-201/203; TLK-202/224; TLK2-209/227/230) and the longest of the
349 short isoforms that lacks the NLS (TLK2-novel-a). After the addition of RA, the expression of
350 the long TLK-202/224 isoform is rapidly downregulated (Figure 3B,C). The subsequent
351 addition of BDNF in serum-free media induced an upregulation of the shortest variants (TLK2-
352 novel-b and -c) and a concomitant downregulation of the longer isoforms. At the end of the
353 differentiation protocol, the TLK2 isoform profile was a broader mix of long and short variants
354 with similar levels of expression (Figure 3B).
355
356 To establish the corresponding pattern of TLK2 isoform protein expression during
357 differentiation, SH-SY5Y whole cell lysates from the timecourse experiment were subjected to
358 immunoblotting with a C-terminal reactive antibody, for which the epitope is predicted to be
359 present in all major splice variants of TLK2 (Figure 4A). Based on the predicted molecular
360 weight of the proteins encoded by the TLK2 transcripts identified in SH-SY5Y cells (see Figure
361 3B), we expected that the long isoforms would migrate in the range 78-87 kDa, while the
362 shorter isoforms lacking the NLS would migrate at 68-75 kDa. Indeed, two groups of bands
363 were observed at approximately 85 kDa and 70 kDa, and their expression was regulated during
364 SH-SY5Y differentiation, broadly correlating with the expression of the long and short TLK2-
365 transcripts observed in Figure 3. Quantification of replicate immunoblots by densitometry
366 revealed that the 85 kDa band had a biphasic expression during differentiation, which reduced
367 during RA treatment and then stabilised during BDNF treatment (Figure 4A,B). The ~70 kDa
368 band increased in expression during differentiation, with this band becoming the dominant
369 isoform in the fully differentiated cells (Figure 4A,B). Taken together these data suggest that
370 neuronal differentiation enhances expression of a TLK2 isoform that lacks the NLS and is
371 predicted to be cytoplasmic.
372
373 **Cytoplasmic localisation of TLK2 in differentiated neurons**
374 Immunofluorescent staining of SH-SY5Y cells at 1, 4, 9 and 11 days of differentiation with the
375 TLK2 C-terminal antiserum, revealed a time-dependent relocalisation of TLK2 from the nucleus
376 to the cytoplasm (Figure 4C). We quantified its subcellular localisation by measuring the
377 intensity of TLK2 staining in regions of interest within the cytoplasm and nucleus of the cells.
378 The plot of log2(cytoplasm/nucleus) in Figure 4D revealed that TLK2 is significantly enriched
379 in the cytoplasm at day 11 compared to day 1.
380
381 To confirm that TLK2 proteins encoded by splice variants lacking the NLS-containing exon 3
382 localise to the cytoplasm, we generated stable tet-inducible SK-N-SH T-REx-Flp-in cell lines
383 that express either FLAG-TLK2(180-750), corresponding to the predicted protein encoded by
384 Ensembl isoform TLK2-213 or full length FLAG-TLK2 corresponding to the protein product of
385 the canonical Ensembl TLK2 full length isoform (TLK2-203). Following a 48 h induction of TLK2

386 expression with doxycycline in these cell lines, we performed a crude subcellular fractionation
387 (Figure 5B). The cells were subjected to hypotonic lysis and we isolated the pellet (enriched in
388 nuclei) and post-nuclear supernatant. Immunoblotting with antibodies raised to compartment
389 markers, histone H3 and GAPDH, confirmed enrichment of nuclear and cytoplasmic proteins
390 respectively (Figure 5B). The immunostaining of anti-FLAG of the subcellular fractions and in
391 fixed cells demonstrated that the N-terminal truncated kinase was exclusively localised to the
392 cytoplasm, while the full length kinase is predominantly nuclear (Figure 5A,B). Taken together
393 we propose that a cytoplasmic pool of TLK2 increases during neuronal differentiation due to
394 two phenomena: an increase in the expression of a short TLK2 splice variant lacking the NLS
395 and the export of full length TLK2 from the nucleus.
396
397 **Nuclear-cytoplasmic shuttling of TLK2**
398 The nuclear-cytoplasmic transport of TLK2 has been previously reported by Zhang et al (1999)
399 who discovered a yeast 2-hybrid interaction between a 14-3-3**ζ** bait and a C-terminal clone of
400 TLK2 (amino acids 657-750). They found that 14-3-3**ζ** immunoprecipitated from cell lysates
401 with TLK2 and a dominant negative 14-3-3 promoted the nuclear localisation of TLK2 (Zhang
402 et al., 1999). Since 14-3-3 proteins act by binding a phosphorylated motif (Yaffe et al., 1997),
403 we hypothesised that during neuronal differentiation, phosphorylation of TLK2 recruits 14-3-3,
404 thus preventing nuclear import of TLK2 and restricting it to the cytoplasm. Using
405 undifferentiated SH-SY5Y cells, we attempted to mimic these signals to drive cytoplasmic
406 localisation of endogenous TLK2 by stimulating kinase signalling with 100 mM KCl and 10 uM
407 forskolin for 1 h. 100 mM KCl is known to depolarise SH-SY5Y cells, mimicking synaptic
408 activity, and should activate Ca^{2+}-dependent intracellular signalling in addition to the MAP
409 kinase pathway (Corrales et al., 2005). Forskolin, an adenylyl cyclase agonist, stimulates
410 cAMP production and hence activates signalling downstream of PKA (cAMP-dependent
411 protein kinase). Cells treated with KCl and forskolin together caused TLK2 to translocate from
412 the nucleus to the cytoplasm as visualised by immunofluorescence (Figure 5C) and quantified
413 by log2(nucleus/cytoplasm) of TLK2 intensity (Figure 5D). These data suggest the
414 nucleocytoplasmic shuttling of TLK2 that occurs during neuronal differentiation might also be
415 regulated in neurons by activity-dependent signalling.
416
417
418

Discussion

We have undertaken the first characterisation of neuronal TLK2 expression and localisation. We found that TLK2 is expressed in the hippocampus and cerebellum, brain regions that are affected in neurodevelopmental disorders linked with disrupted motor function and cognition. In addition to canonical full length TLK2, we observed splice diversity at the N-terminus of the protein, including variants that lack an NLS. Furthermore, cytoplasmic TLK2 increased during neuronal differentiation, driven by both enhanced expression of TLK2 variants lacking the NLS, and nuclear export of full length TLK2. We also found that the localisation of TLK2 can be regulated acutely by mimicking synaptic activity. Our data suggest future studies into the pathological mechanisms of MRD57 should consider cytoplasmic TLK2 signalling in developing and mature neurons.

Expression and alternative splicing of neuronal TLK2

Our analysis of TLK2 transcripts in mouse brain, SH-SY5Y cells, and publicly available RNAseq datasets revealed broad conservation of full length TLK2 and shorter transcripts lacking N-terminal exons. Interestingly the canonical, and longest, human Ensembl isoform, TLK2-201, comprising 22 exons is weakly expressed, except in aorta and testis (Figure S1), while the most abundant variant in brain and across the body is TLK-202, which lacks exons 5 and 12. Indeed the other major isoforms that are expressed (TLK-203 and TLK-213) also lack exon 12. TLK-213 is the major annotated short isoform that lacks the N-terminus and NLS and is the human homologue of the short mTLK2-207 isoform that was first identified in mouse testis (Shalom and Don, 1999). However, when we assessed the splice diversity of TLK2 transcripts in SH-SY5Y cells during neuronal differentiation we failed to observe TLK2-213, but instead discovered several novel isoforms that lack the NLS encoded by exon 3. These variants were only weakly detected in HEK293 cDNA, suggesting they might be upregulated in neurons. When we immunoblotted TLK2 in SH-SY5Y cells using an antibody with a C-terminal epitope, we observed bands that broadly correspond to long and short isoforms. However, due to the minor differences in molecular mass arising from the various splicing events it is not possible to correlate specific protein bands with specific splice variants.

Interestingly, human TLK1, which shares 78% homology with full length TLK2, also possesses a short isoform, TLK1B, lacking the N-terminus and hence the NLS. Constitutive expression of TLK1B is highest in testis, liver and lung, but low in brain (Li et al., 2001). Furthermore, TLK1B expression can be induced by genotoxic stress, such as ionising radiation, through translational regulation of an alternative start site (Li et al., 2001). Surprisingly, in contrast to short TLK2, TLK1B localises to the nucleus where it coordinates DNA repair, even in the absence of the TLK1 NLS (Li et al., 2001; Sunavala-Dossabhoy et al., 2005), suggesting TLK1B is targeted to the nucleus by an alternative mechanism.

Using splice junction-specific *in situ* probes, we were able to examine the relative distributions of long and short TLK2 isoforms in the mouse brain. TLK2 was expressed in the major cell types of the hippocampus and cerebellum, although it was notable that expression in excitatory neurons was easily observed, but inhibitory interneurons were not detectably stained. This is in contradiction to single cell RNAseq analyses of mouse hippocampus and cerebellum, which detected abundant TLK2 transcripts in various interneuron cell types (Habib et al., 2016; Kozareva et al., 2021). We observed differential expression of TLK2 isoforms in excitatory cell types of the hippocampal formation, with intriguing differences

467 between CA1 and CA3 intensity (mTLK2-204) and the blades that comprise the dentate
468 gyrus (mTLK2-201). It is not surprising that there are transcriptional differences between
469 hippocampal cell types, which presumably define their function. However, a deeper
470 understanding of the role of TLK2 in the developing and mature brain is needed to predict the
471 significance of these data.
472
473 **Neuronal differentiation- and activity-dependent nucleocytoplasmic shuttling of TLK2**
474 We observed a striking loss of nuclear TLK2 staining in SH-SY5Y cells during neuronal
475 differentiation. Since we did not observe a significant concomitant reduction in protein
476 expression of longer TLK2 isoforms, we concluded that TLK2 was shuttling from the nucleus
477 to the cytoplasm during differentiation. The upregulation of short TLK2 isoform expression we
478 observed is also likely to contribute to the enhancement of cytoplasmic TLK2. This was
479 validated by creating stable SK-N-SH cells cell lines expressing an N-terminally truncated
480 TLK2 variant, which was confined to the cytoplasm. These data agree with the non-nuclear
481 localisation of a short TLK2 variant that was overexpressed in AD293 cells (Mortuza et al.,
482 2018).
483
484 Our observation of long TLK2 export from the nucleus during differentiation is consistent with
485 previous data on the cytoplasmic and nuclear distribution of TLK2. Using a C-terminal TLK2
486 monoclonal antibody, Zhang et al (1999) demonstrated cell cycle-dependent shuttling of
487 TLK2 in cultures of synchronised 3T3 cells. During G1 phase, TLK2 was predominantly
488 outside the nucleus and co-localised with vimentin, an intermediate filament protein. With the
489 onset of S-phase TLK2 was observed to localise to the nuclear periphery and then within the
490 nucleus during late G2 (Zhang et al., 1999). Thus, the nuclear export and cytoplasmic
491 accumulation of TLK2 during neuronal differentiation correlates with these cells exiting the
492 cell cycle. Mechanistically, Zhang et al. attributed the nucleocytoplasmic shuttling of TLK2 to
493 an interaction with 14-3-3 proteins, with binding preventing TLK2 nuclear import. They
494 identified a putative 14-3-3 interaction motif in the C-terminus (amino acids 747-753). Serine
495 phosphorylation of 14-3-3 motifs is required for binding, but the phosphorylation of that motif
496 in TLK2 has not been characterised. Since we observed translocation of TLK2 in response to
497 KCl-induced depolarisation and FSK, it is possible that phosphorylation of TLK2 by a Ca^{2+}-
498 and/or cAMP-dependent kinase facilitates 14-3-3 binding and hence retains it in the
499 cytoplasm. There are examples in the literature of transcription factors that require neuronal
500 activity-dependent Ca^{2+} and cAMP signalling for nucleocytoplasmic shuttling, such as the
501 transcriptional activator CRTC1 (Ch'ng et al., 2012). The functions of non-nuclear TLK2 have
502 not been investigated, although its colocalisation with vimentin might suggest regulation of
503 the cytoskeleton (Zhang et al., 1999). This is in-line with the Tousled homologue in
504 *Drosophila*, which has been shown to genetically interact with *rho1* (Gregory et al., 2007), a
505 cytoskeletal regulator, and the *tlk* mutant has altered microtubule and actin filament density
506 in developing follicle cells (Yeh et al., 2015). Other cytoplasmic TLK2 interactors are lacking.
507 Previous TLK2 immunoprecipitation or proximal interactome studies have been conducted in
508 non-neuronal proliferating cell lines, where it might be expected that TLK2 is predominantly
509 nuclear, and these have tended to identify nuclear binding partners (Pavinato et al., 2022;
510 Segura-Bayona et al., 2017).
511
512 **The implications of neuronal TLK2 splice variants for MRD57**
513 Our study raises mechanistic questions about the pathology of the neurodevelopmental
514 disorder MRD57, in which patients are haploinsufficient for TLK2, predominantly through *de*

novo mutations (Lelieveld et al., 2016; Pavinato et al., 2022; Reijnders et al., 2018; Woods et al., 2022). The important role of TLK2 in cell cycle regulation and DNA repair has led to the hypothesis that the proliferation and differentiation of neural progenitors is affected in MRD57 patient brain development (Segura-Bayona and Stracker, 2019). MRD57 phenotypes are presumably due to processes involving TLK2 that are not compensated by TLK1, such as non-nuclear functions in post-mitotic neurons. Surprisingly, the TLK2 knockout mouse did not display any cell cycle defects, due to compensation by TLK1, except in the placenta where TLK1 expression is low (Segura-Bayona et al., 2017). However, the knockout mouse might not be a good model for MRD57 as there were no reported brain or behavioural anomalies in the TLK2 conditional heterozygous or homozygous mutant mice (Segura-Bayona et al., 2017).

It is notable that MRD57 patient missense mutations have not been identified in exons 2, 4-7 or 12. This suggests that these regions are either not necessary for TLK2 function, or their mutation is tolerated through compensation by alternative splice variants lacking these exons. Relevant to our study, one patient has been identified with a homozygous substitution mutation (K55E) adjacent to the NLS (Töpf et al., 2020), and it would be interesting to study the localisation and nuclear shuttling of this TLK2 mutant in neurons. Furthermore, future studies of neuronal TLK2 should focus on identifying its neuronal cytoplasmic substrates to advance our understanding of TLK2 in developing and mature neurons and the pathology of MRD57.

Conflict of interest statement

The authors declare that the research was conducted in the absence of any commercial or financial relationships that could be construed as a potential conflict of interest

Credit author statement

Lubna Nuhu-Soso: Writing – review & editing, Writing – original draft, Visualization, Methodology, Investigation, Formal analysis, Conceptualization. **Heidi Denton**: Investigation, Methodology, Formal analysis. **Darren L. Goffin**: Supervision, Writing – review & editing, Methodology, Conceptualization. **Ines Hahn**: Writing – review & editing, Supervision, Funding acquisition.
Gareth J.O. Evans: Writing – review & editing, Writing – original draft, Visualization, Supervision, Project administration, Methodology, Funding acquisition, Formal analysis, Data curation, Conceptualization.

Funding

This work was part-funded by the Wellcome Trust (ref: 204829) to GJOE and DLG through the Centre for Future Health (CFH) at the University of York, and by an Academy of Medical Science Springboard Award to IH (SBF008\1140).

Acknowledgements

We are grateful to Prof Betsy Pownall and Dr Harry Isaacs (University of York) for valuable advice regarding the *in situ* hybridisation experiments. We thank the Bioscience Technology Facility at the University of York for providing access to confocal microscopes.

560 **References**

561 Bhoir, S., De Benedetti, A., 2023. Targeting prostate cancer, the “tousled way.” Int. J. Mol.
562 Sci. 24, 11100. https://doi.org/10.3390/ijms241311100
563 Bruinsma, W., van den Berg, J., Aprelia, M., Medema, R.H., 2016. Tousled-like kinase 2
564 regulates recovery from a DNA damage-induced G2 arrest. EMBO Rep. 17, 659–670.
565 https://doi.org/10.15252/embr.201540767
566 Ch’ng, T.H., Uzgil, B., Lin, P., Avliyakulov, N.K., O’Dell, T.J., Martin, K.C., 2012. Activity-
567 dependent transport of the transcriptional coactivator CRTC1 from synapse to nucleus.
568 Cell 150, 207–221. https://doi.org/10.1016/j.cell.2012.05.027
569 Corrales, A., Montoya G, J.V., Sutachan, J.-J., Cornillez-Ty, G., Garavito-Aguilar, Z., Xu, F.,
570 Blanck, T.J.J., Recio-Pinto, E., 2005. Transient increases in extracellular K+ produce
571 two pharmacological distinct cytosolic Ca2+ transients. Brain Res. 1031, 174–184.
572 https://doi.org/10.1016/j.brainres.2004.10.031
573 Encinas, M., Iglesias, M., Liu, Y., Wang, H., Muhaisen, A., Ceña, V., Gallego, C., Comella,
574 J.X., 2000. Sequential treatment of SH-SY5Y cells with retinoic acid and brain-derived
575 neurotrophic factor gives rise to fully differentiated, neurotrophic factor-dependent,
576 human neuron-like cells. J. Neurochem. 75, 991–1003. https://doi.org/10.1046/j.1471-
577 4159.2000.0750991.x
578 Fisher, M.E., Isaacs, H.V., Pownall, M.E., 2002. eFGF is required for activation of XmyoD
579 expression in the myogenic cell lineage of Xenopus laevis. Development 129, 1307–
580 1315. https://doi.org/10.1242/dev.129.6.1307
581 Gregory, S.L., Shandala, T., O’Keefe, L., Jones, L., Murray, M.J., Saint, R., 2007. A
582 Drosophila overexpression screen for modifiers of Rho signalling in cytokinesis. Fly 1,
583 13–22. https://doi.org/10.4161/fly.3806
584 Habib, N., Li, Y., Heidenreich, M., Swiech, L., Avraham-Davidi, I., Trombetta, J.J., Hession,
585 C., Zhang, F., Regev, A., 2016. Div-Seq: Single-nucleus RNA-Seq reveals dynamics of
586 rare adult newborn neurons. Science 353, 925–928.
587 https://doi.org/10.1126/science.aad7038
588 Harrison, P.W., Amode, M.R., Austine-Orimoloye, O., Azov, A.G., Barba, M., Barnes, I.,
589 Becker, A., Bennett, R., Berry, A., Bhai, J., Bhurji, S.K., Boddu, S., Branco Lins, P.R.,
590 Brooks, L., Ramaraju, S.B., Campbell, L.I., Martinez, M.C., Charkhchi, M., Chougule, K.,
591 Cockburn, A., Davidson, C., De Silva, N.H., Dodiya, K., Donaldson, S., El Houdaigui, B.,
592 Naboulsi, T.E., Fatima, R., Giron, C.G., Genez, T., Grigoriadis, D., Ghattaoraya, G.S.,
593 Martinez, J.G., Gurbich, T.A., Hardy, M., Hollis, Z., Hourlier, T., Hunt, T., Kay, M.,
594 Kaykala, V., Le, T., Lemos, D., Lodha, D., Marques-Coelho, D., Maslen, G., Merino,
595 G.A., Mirabueno, L.P., Mushtaq, A., Hossain, S.N., Ogeh, D.N., Sakthivel, M.P., Parker,
596 A., Perry, M., Piližota, I., Poppleton, D., Prosovetskaia, I., Raj, S., Pérez-Silva, J.G.,
597 Salam, A.I.A., Saraf, S., Saraiva-Agostinho, N., Sheppard, D., Sinha, S., Sipos, B.,
598 Sitnik, V., Stark, W., Steed, E., Suner, M.-M., Surapaneni, L., Sutinen, K., Tricomi, F.F.,
599 Urbina-Gómez, D., Veidenberg, A., Walsh, T.A., Ware, D., Wass, E., Willhoft, N.L.,
600 Allen, J., Alvarez-Jarreta, J., Chakiachvili, M., Flint, B., Giorgetti, S., Haggerty, L., Ilsley,
601 G.R., Keatley, J., Loveland, J.E., Moore, B., Mudge, J.M., Naamati, G., Tate, J.,
602 Trevanion, S.J., Winterbottom, A., Frankish, A., Hunt, S.E., Cunningham, F., Dyer, S.,
603 Finn, R.D., Martin, F.J., Yates, A.D., 2024. Ensembl 2024. Nucleic Acids Res. 52, D891–
604 D899. https://doi.org/10.1093/nar/gkad1049
605 Kim, J.-A., Anurag, M., Veeraraghavan, J., Schiff, R., Li, K., Wang, X.-S., 2016a.
606 Amplification of TLK2 Induces Genomic Instability via Impairing the G2-M Checkpoint.
607 Mol. Cancer Res. 14, 920–927. https://doi.org/10.1158/1541-7786.MCR-16-0161
608 Kim, J.-A., Tan, Y., Wang, X., Cao, X., Veeraraghavan, J., Liang, Y., Edwards, D.P., Huang,
609 S., Pan, X., Li, K., Schiff, R., Wang, X.-S., 2016b. Comprehensive functional analysis of
610 the tousled-like kinase 2 frequently amplified in aggressive luminal breast cancers. Nat.
611 Commun. 7, 12991. https://doi.org/10.1038/ncomms12991
612 Klimovskaia, I.M., Young, C., Strømme, C.B., Menard, P., Jasencakova, Z., Mejlvang, J.,
613 Ask, K., Ploug, M., Nielsen, M.L., Jensen, O.N., Groth, A., 2014. Tousled-like kinases

614 phosphorylate Asf1 to promote histone supply during DNA replication. Nat. Commun. 5,
615 3394. https://doi.org/10.1038/ncomms4394
616 Kozareva, V., Martin, C., Osorno, T., Rudolph, S., Guo, C., Vanderburg, C., Nadaf, N.,
617 Regev, A., Regehr, W.G., Macosko, E., 2021. A transcriptomic atlas of mouse cerebellar
618 cortex comprehensively defines cell types. Nature 598, 214–219.
619 https://doi.org/10.1038/s41586-021-03220-z
620 Lee, S.-B., Segura-Bayona, S., Villamor-Payà, M., Saredi, G., Todd, M.A.M., Attolini, C.S.-
621 O., Chang, T.-Y., Stracker, T.H., Groth, A., 2018. Tousled-like kinases stabilize
622 replication forks and show synthetic lethality with checkpoint and PARP inhibitors. Sci
623 Adv 4, eaat4985. https://doi.org/10.1126/sciadv.aat4985
624 Lelieveld, S.H., Reijnders, M.R.F., Pfundt, R., Yntema, H.G., Kamsteeg, E.-J., de Vries, P.,
625 de Vries, B.B.A., Willemsen, M.H., Kleefstra, T., Löhner, K., Vreeburg, M., Stevens,
626 S.J.C., van der Burgt, I., Bongers, E.M.H.F., Stegmann, A.P.A., Rump, P., Rinne, T.,
627 Nelen, M.R., Veltman, J.A., Vissers, L.E.L.M., Brunner, H.G., Gilissen, C., 2016. Meta-
628 analysis of 2,104 trios provides support for 10 new genes for intellectual disability. Nat.
629 Neurosci. 19, 1194–1196. https://doi.org/10.1038/nn.4352
630 Li, Y., DeFatta, R., Anthony, C., Sunavala, G., De Benedetti, A., 2001. A translationally
631 regulated Tousled kinase phosphorylates histone H3 and confers radioresistance when
632 overexpressed. Oncogene 20, 726–738. https://doi.org/10.1038/sj.onc.1204147
633 López-Rivera, J.A., Pérez-Palma, E., Symonds, J., Lindy, A.S., McKnight, D.A., Leu, C.,
634 Zuberi, S., Brunklaus, A., Møller, R.S., Lal, D., 2020. A catalogue of new incidence
635 estimates of monogenic neurodevelopmental disorders caused by de novo variants.
636 Brain 143, 1099–1105. https://doi.org/10.1093/brain/awaa051
637 Mortuza, G.B., Hermida, D., Pedersen, A.-K., Segura-Bayona, S., López-Méndez, B.,
638 Redondo, P., Rüther, P., Pozdnyakova, I., Garrote, A.M., Muñoz, I.G., Villamor-Payà,
639 M., Jauset, C., Olsen, J.V., Stracker, T.H., Montoya, G., 2018. Molecular basis of
640 Tousled-Like Kinase 2 activation. Nat. Commun. 9, 2535.
641 https://doi.org/10.1038/s41467-018-04941-y
642 Pavinato, L., Villamor-Payà, M., Sanchiz-Calvo, M., Andreoli, C., Gay, M., Vilaseca, M.,
643 Arauz-Garofalo, G., Ciolfi, A., Bruselles, A., Pippucci, T., Prota, V., Carli, D., Giorgio, E.,
644 Radio, F.C., Antona, V., Giuffrè, M., Ranguin, K., Colson, C., De Rubeis, S., Dimartino,
645 P., Buxbaum, J.D., Ferrero, G.B., Tartaglia, M., Martinelli, S., Stracker, T.H., Brusco, A.,
646 2022. Functional analysis of TLK2 variants and their proximal interactomes implicates
647 impaired kinase activity and chromatin maintenance defects in their pathogenesis. J.
648 Med. Genet. 59, 170–179. https://doi.org/10.1136/jmedgenet-2020-107281
649 Reijnders, M.R.F., Miller, K.A., Alvi, M., Goos, J.A.C., Lees, M.M., de Burca, A., Henderson,
650 A., Kraus, A., Mikat, B., de Vries, B.B.A., Isidor, B., Kerr, B., Marcelis, C., Schluth-
651 Bolard, C., Deshpande, C., Ruivenkamp, C.A.L., Wieczorek, D., Deciphering
652 Developmental Disorders Study, Baralle, D., Blair, E.M., Engels, H., Lüdecke, H.-J.,
653 Eason, J., Santen, G.W.E., Clayton-Smith, J., Chandler, K., Tatton-Brown, K., Payne, K.,
654 Helbig, K., Radtke, K., Nugent, K.M., Cremer, K., Strom, T.M., Bird, L.M., Sinnema, M.,
655 Bitner-Glindzicz, M., van Dooren, M.F., Alders, M., Koopmans, M., Brick, L., Kozenko,
656 M., Harline, M.L., Klaassens, M., Steinraths, M., Cooper, N.S., Edery, P., Yap, P.,
657 Terhal, P.A., van der Spek, P.J., Lakeman, P., Taylor, R.L., Littlejohn, R.O., Pfundt, R.,
658 Mercimek-Andrews, S., Stegmann, A.P.A., Kant, S.G., McLean, S., Joss, S.,
659 Swagemakers, S.M.A., Douzgou, S., Wall, S.A., Küry, S., Calpena, E., Koelling, N.,
660 McGowan, S.J., Twigg, S.R.F., Mathijssen, I.M.J., Nellaker, C., Brunner, H.G., Wilkie,
661 A.O.M., 2018. De Novo and Inherited Loss-of-Function Variants in TLK2: Clinical and
662 Genotype-Phenotype Evaluation of a Distinct Neurodevelopmental Disorder. Am. J.
663 Hum. Genet. 102, 1195–1203. https://doi.org/10.1016/j.ajhg.2018.04.014
664 Roe, J.L., Rivin, C.J., Sessions, R.A., Feldmann, K.A., Zambryski, P.C., 1993. The Tousled
665 gene in A. thaliana encodes a protein kinase homolog that is required for leaf and flower
666 development. Cell 75, 939–950. https://doi.org/10.1016/0092-8674(93)90537-z
667 RStudio Team, 2020. RStudio Integrated Development for R. http://www.rstudio.com/.
668 Schindelin, J., Arganda-Carreras, I., Frise, E., Kaynig, V., Longair, M., Pietzsch, T.,

Preibisch, S., Rueden, C., Saalfeld, S., Schmid, B., Tinevez, J.-Y., White, D.J., Hartenstein, V., Eliceiri, K., Tomancak, P., Cardona, A., 2012. Fiji: an open-source platform for biological-image analysis. Nat. Methods 9, 676–682. https://doi.org/10.1038/nmeth.2019

Segura-Bayona, S., Knobel, P.A., González-Burón, H., Youssef, S.A., Peña-Blanco, A., Coyaud, É., López-Rovira, T., Rein, K., Palenzuela, L., Colombelli, J., Forrow, S., Raught, B., Groth, A., de Bruin, A., Stracker, T.H., 2017. Differential requirements for Tousled-like kinases 1 and 2 in mammalian development. Cell Death Differ. 24, 1872–1885. https://doi.org/10.1038/cdd.2017.108

Segura-Bayona, S., Stracker, T.H., 2019. The Tousled-like kinases regulate genome and epigenome stability: implications in development and disease. Cell. Mol. Life Sci. 76, 3827–3841. https://doi.org/10.1007/s00018-019-03208-z

Shalom, S., Don, J., 1999. Tlk, a novel evolutionarily conserved murine serine threonine kinase, encodes multiple testis transcripts. Mol. Reprod. Dev. 52, 392–405. https://doi.org/10.1002/(SICI)1098-2795(199904)52:4<392::AID-MRD8>3.0.CO;2-Y

Silljé, H.H., Takahashi, K., Tanaka, K., Van Houwe, G., Nigg, E.A., 1999. Mammalian homologues of the plant Tousled gene code for cell-cycle-regulated kinases with maximal activities linked to ongoing DNA replication. EMBO J. 18, 5691–5702. https://doi.org/10.1093/emboj/18.20.5691

Sjöstedt, E., Zhong, W., Fagerberg, L., Karlsson, M., Mitsios, N., Adori, C., Oksvold, P., Edfors, F., Limiszewska, A., Hikmet, F., Huang, J., Du, Y., Lin, L., Dong, Z., Yang, L., Liu, X., Jiang, H., Xu, X., Wang, J., Yang, H., Bolund, L., Mardinoglu, A., Zhang, C., von Feilitzen, K., Lindskog, C., Pontén, F., Luo, Y., Hökfelt, T., Uhlén, M., Mulder, J., 2020. An atlas of the protein-coding genes in the human, pig, and mouse brain. Science 367, eaay5947. https://doi.org/10.1126/science.aay5947

Sunavala-Dossabhoy, G., Balakrishnan, S.K., Sen, S., Nuthalapaty, S., De Benedetti, A., 2005. The radioresistance kinase TLK1B protects the cells by promoting repair of double strand breaks. BMC Mol. Biol. 6, 19. https://doi.org/10.1186/1471-2199-6-19

Töpf, A., Oktay, Y., Balaraju, S., Yilmaz, E., Sonmezler, E., Yis, U., Laurie, S., Thompson, R., Roos, A., MacArthur, D.G., Yaramis, A., Güngör, S., Lochmüller, H., Hiz, S., Horvath, R., 2020. Severe neurodevelopmental disease caused by a homozygous TLK2 variant. Eur. J. Hum. Genet. 28, 383–387. https://doi.org/10.1038/s41431-019-0519-x

Villamor-Payà, M., Sanchiz-Calvo, M., Smak, J., Pais, L., Sud, M., Shankavaram, U., Lovgren, A.K., Austin-Tse, C., Ganesh, V.S., Gay, M., Vilaseca, M., Arauz-Garofalo, G., Palenzuela, L., VanNoy, G., O'Donnell-Luria, A., Stracker, T.H., 2024. De novo TLK1 and MDM1 mutations in a patient with a neurodevelopmental disorder and immunodeficiency. iScience 27, 109984. https://doi.org/10.1016/j.isci.2024.109984

Woods, E., Spiller, M., Balasubramanian, M., 2022. Report of two children with global developmental delay in association with de novo TLK2 variant and literature review. Am. J. Med. Genet. A 188, 931–940. https://doi.org/10.1002/ajmg.a.62580

Yaffe, M.B., Rittinger, K., Volinia, S., Caron, P.R., Aitken, A., Leffers, H., Gamblin, S.J., Smerdon, S.J., Cantley, L.C., 1997. The structural basis for 14-3-3:phosphopeptide binding specificity. Cell 91, 961–971. https://doi.org/10.1016/s0092-8674(00)80487-0

Yamakawa, A., Kameoka, Y., Hashimoto, K., Yoshitake, Y., Nishikawa, K., Tanihara, K., Date, T., 1997. cDNA cloning and chromosomal mapping of genes encoding novel protein kinases termed PKU-alpha and PKU-beta, which have nuclear localization signal. Gene 202, 193–201. https://doi.org/10.1016/s0378-1119(97)00495-2

Yeh, T.-H., Huang, S.-Y., Lan, W.-Y., Liaw, G.-J., Yu, J.-Y., 2015. Modulation of cell morphogenesis by tousled-like kinase in the Drosophila follicle cell. Dev. Dyn. 244, 852–865. https://doi.org/10.1002/dvdy.24292

Zhang, S., Xing, H., Muslin, A.J., 1999. Nuclear localization of protein kinase U-alpha is regulated by 14-3-3. J. Biol. Chem. 274, 24865–24872. https://doi.org/10.1074/jbc.274.35.24865

723 **Figure legends**
724
725 Figure 1. TLK2 has splice variant diversity in the human brain. (A) Exonic structure of human
726 TLK2, mapped onto a schematic representation of its protein domains. NLS, nuclear
727 localisation sequence; CC, coiled-coil domain. (B) Table of % TLK2 transcript abundance in
728 the human hippocampus and cerebellum derived from GTEx RNAseq data. Exons and
729 transcripts labelled in red are predicted to be non-protein coding. Only transcripts present >2%
730 in either brain region are included.
731
732 Figure 2. Multiple isoforms of TLK2 are expressed in mouse forebrain and cerebellum.
733 (A) RT-PCR of TLK2 splice variants from mouse forebrain and cerebellum cDNA. Transcript
734 specific primer pairs or pan exon 1-6 primers. (B) Left, lane from PCR of exon 1-6 primer
735 pair. The four bands were excised and sequenced. Right, exon structure of sequenced
736 mouse brain splice variants, and location of *in situ* hybridisation probes. *In situ* hybridisation
737 was performed on 25 µm frozen sections from coronal (C) or sagittal (E) P56 mouse brain
738 sections. The indicated 150 bp exon junction spanning probes were used to examine
739 calbindin or TLK2 transcript expression in the hippocampus (C) or cerebellar cortex (E).
740 Representative images are shown from n=3 sections from two mouse brains. Cerebellar
741 cortex images are shown at x10 and x40 magnification, indicated by the insert box. DG,
742 dentate gyrus; ML, molecular layer; GL, granule layer; PCL, Purkinje cell layer. Scale bars:
743 hippocampus 100 µm, cerebellar cortex x10, 200 µm; x40, 20 µm. (D**)** Heatmap depicting
744 quantification of TLK2 splice variant expression within the dentate gyrus, CA1 and CA3 sub-
745 regions of the hippocampal formation. For each section, pixel intensity was measured in
746 regions of interest (ROI), as indicated in the cartoon and normalised to the ROI located in the
747 suprapyramidal blade of the dentate gyrus. Three sections were quantified for each probe.
748
749 Figure 3. Alternative splicing of TLK2 is regulated during neuronal differentiation. SH-SY5Y
750 cultures were differentiated by sequential treatment with retinoic acid (RA) and brain derived
751 neurotrophic factor (BDNF) as described in Materials and Methods. (A) Brightfield images of
752 SH-SY5Y cultures at the indicated days of differentiation. Scale bar = 40 µm. (B) cDNA was
753 prepared from SH-SY5Y cells at the indicated time points, and HEK293 cells (control) and
754 subjected to PCR with primers for exons 1 and 9 of human TLK2, Tau, and GAPDH. The six
755 TLK2 bands obtained from the cells were excised and subjected to Sanger sequencing. The
756 right hand schematic summarises the exon structure of each sequence and any
757 corresponding Ensembl transcripts that these align to and the predicted molecular mass of
758 the encoded protein. The bottom plot presents quantitative densitometry of each TLK2 RT-
759 PCR product, expressed as a percentage of the total intensity at each timepoint.
760
761 Figure 4. Neuronal differentiation alters the nuclear-cytoplasmic distribution of TLK2. SH-
762 SY5Y cells were lysed or fixed at the indicated timepoints during neuronal differentiation and
763 subjected to immunoblotting with anti-TLK2, anti-β3-tubulin or anti-actin (A) or
764 immunocytochemistry with anti-TLK2 (1:1000; green) and DAPI staining (purple) Scale bar =
765 10 µm. (C). (B) Quantification of TLK2 immunoblot band intensity from (A), data plotted as
766 stacked bars and raw data points for long TLK2 (yellow circles) and short TLK2 (green
767 circles) isoforms. Data were normalised to the intensity of actin and then day 4 short TLK2
768 (n=3 independent experiments). (D) TLK2 intensity was measured in regions of interest in the
769 nucleus and cytoplasm of 100 cells from each timepoint (n=3 independent experiments).
770 Data are plotted as $\log_2$(nuclear/cytoplasmic) TLK2 intensity at each timepoint (grey filled

771 circles). Hollow black circles represent the mean of each replicate. For (B) and (D), data
772 were analysed by Kruskal-Wallis two-tailed ANOVA and Dunn's post-hoc test; * $p < 0.05$; ** p
773 < 0.01 compared to day 1. For significance in (B), * = long TLK2 and # = short TLK2.
774
775 Figure 5. Activity-dependent redistribution of TLK2. Inducible Flp-in SK-N-SH cells
776 expressing FLAG-tagged long TLK2-203 or short TLK2-213 were treated with or without 1
777 µg/ml doxycycline (dox) for 48 h. (A) Representative immunofluorescence images of dox-
778 treated cells stained with anti-FLAG (1:1000) and DAPI. Scale bar = 10 µm. (B) Cells plated
779 in dishes were lysed and subject to subcellular fractionation to yield a nuclear pellet and
780 postnuclear supernatant. The samples were subjected to immunoblotting with anti-FLAG,
781 anti-GAPDH and anti-histone H3. (C) SH-SY5Y cells equilibrated in KREBS buffer were
782 incubated for 1 h in KREBS buffer with or without (control) 100 mM KCl and 10 µM forskolin
783 (FSK). Fixed cells were stained with anti-TLK2 and DAPI. Scale bar = 10 µm. (D) TLK2
784 intensity was measured in regions of interest in the nucleus and cytoplasm of 100 cells from
785 each treatment (n=3 experiments). Data are plotted as $\log_2$(nuclear/cytoplasmic) TLK2
786 intensity at each timepoint (grey filled circles). Hollow black circles represent the mean of
787 each replicate and were analysed by t- test; * $p < 0.05$ compared to control.
788

Figure 1

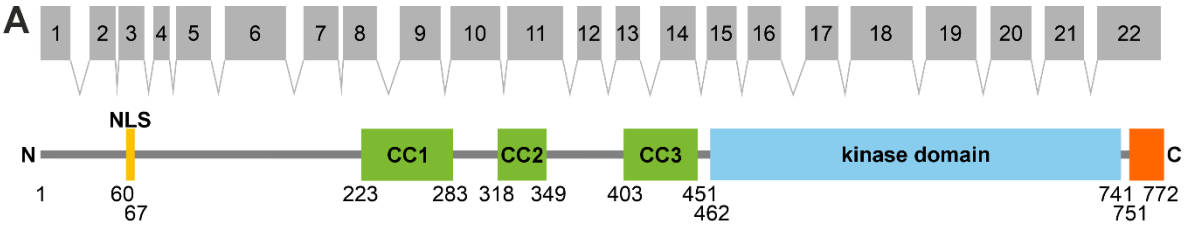

B

TLK2 exon structure	human RNAseq (GTEx) Ensembl transcript	% HC	% CBM
1 2 3 4 5 6 7 8-9 10 11 12 13-14 15-21 22	TLK2-201	2	2.1
1 2 3 4 6 7 8-9 10 11 13-14 15-21 22	TLK2-202	37.2	39
1 2 3 4 5 6 7 8-9 10 11 13-14 15-21 22	TLK2-203	2.5	5.6
22	TLK2-207	29	28
1 X 2 3 4 5 6a 6b 7 8-9 10 11 13-14 15-21 22	TLK2-213	22.5	12.8
21 22	TLK2-214	1.4	6.1

red exon/transcript = non-coding

Figure 2

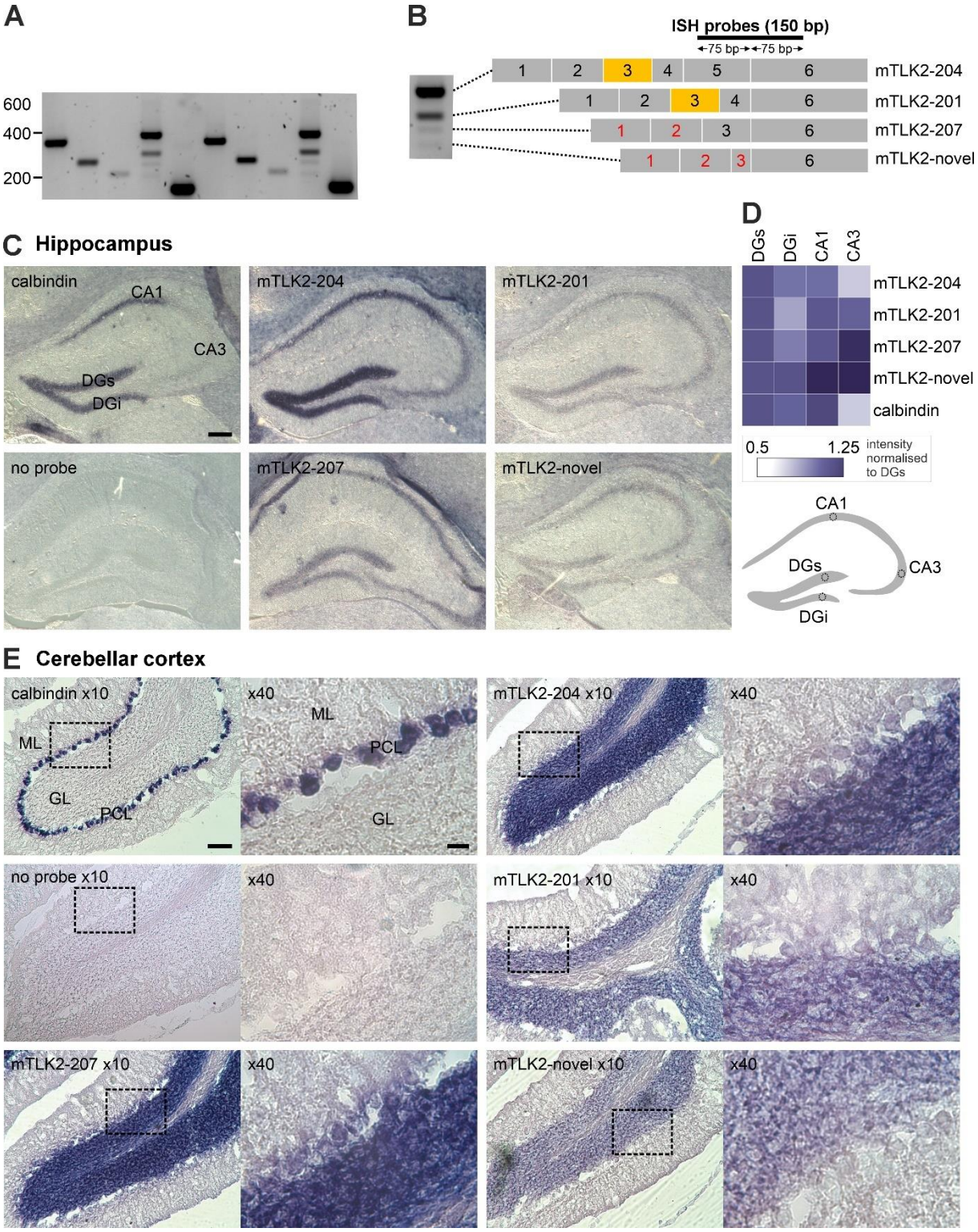
A
600
400
200
B
ISH probes (150 bp)
75 bp
75 bp
1 2 3 4 5 6 mTLK2-204
1 2 3 4 6 mTLK2-201
1 2 3 6 mTLK2-207
1 2 3 6 mTLK2-novel
C Hippocampus
calbindin
CA1
CA3
DGs
DGi
mTLK2-204
mTLK2-201
no probe
mTLK2-207
mTLK2-novel
D
DGs
DGi
CA1
CA3
mTLK2-204
mTLK2-201
mTLK2-207
mTLK2-novel
calbindin
0.5
1.25
intensity normalised to DGs
CA1
DGs
CA3
DGi
E Cerebellar cortex
calbindin x10
x40
ML
PCL
GL
mTLK2-204 x10
no probe x10
mTLK2-201 x10
mTLK2-207 x10
mTLK2-novel x10

Figure 3

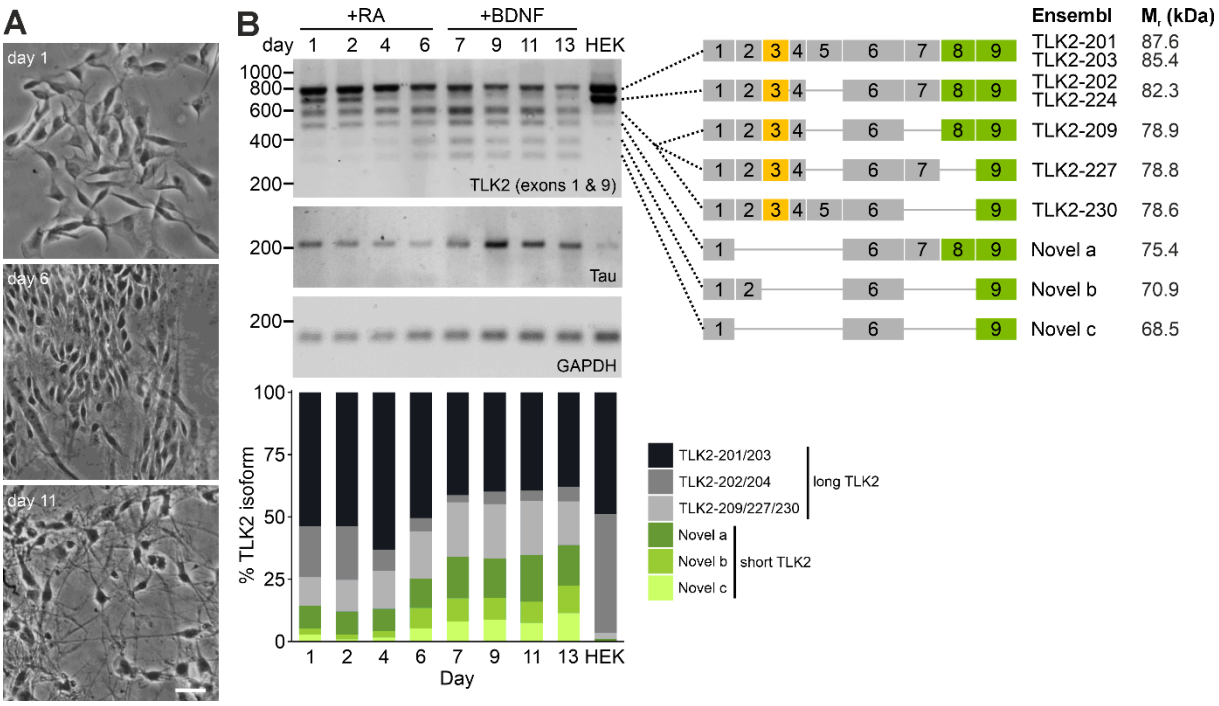
A
day 1
day 6
day 11
B
+RA
+BDNF
day 1 2 4 6 7 9 11 13 HEK
1000
800
600
400
200
TLK2 (exons 1 & 9)
200
Tau
200
GAPDH
100
75
50
25
0
% TLK2 isoform
1 2 4 6 7 9 11 13 HEK
Day
TLK2-201/203
TLK2-202/204
TLK2-209/227/230
long TLK2
Novel a
Novel b
Novel c
short TLK2
Ensembl
Mr (kDa)
TLK2-201 87.6
TLK2-203 85.4
TLK2-202
TLK2-224 82.3
TLK2-209 78.9
TLK2-227 78.8
TLK2-230 78.6
Novel a 75.4
Novel b 70.9
Novel c 68.5

Figure 4

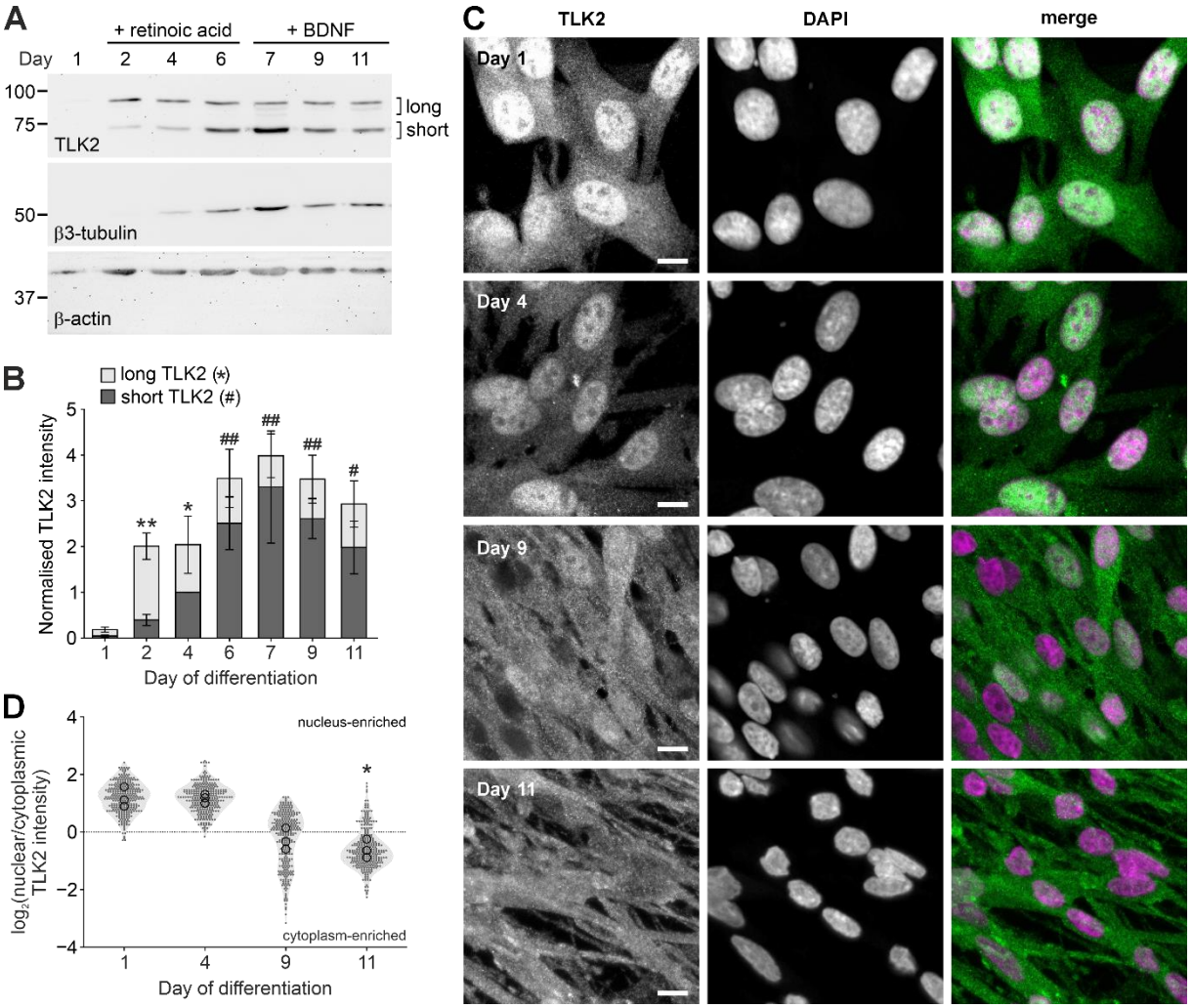
A
+ retinoic acid
+ BDNF
Day 1 2 4 6 7 9 11
100
75
TLK2
] long
] short
50
β3-tubulin
37
β-actin
B
long TLK2 (*)
short TLK2 (#)
Normalised TLK2 intensity
Day of differentiation
C
TLK2
DAPI
merge
Day 1
Day 4
Day 9
Day 11
D
nucleus-enriched
cytoplasm-enriched
log2(nuclear/cytoplasmic TLK2 intensity)
Day of differentiation

Figure 5

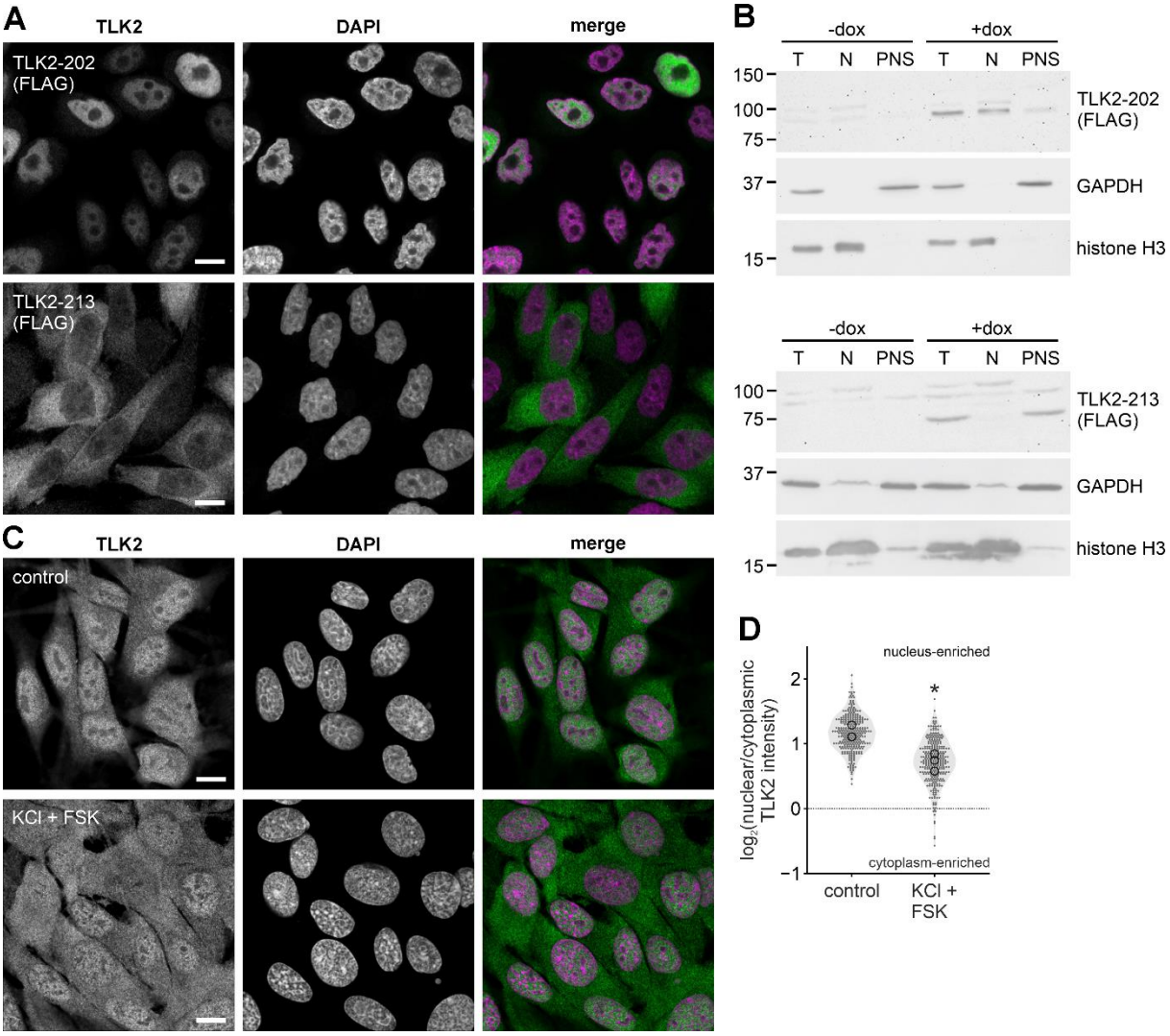
A
TLK2
DAPI
merge
TLK2-202 (FLAG)
TLK2-213 (FLAG)
B
-dox
+dox
T N PNS T N PNS
150
100
75
37
15
TLK2-202 (FLAG)
GAPDH
histone H3
TLK2-213 (FLAG)
C
control
KCl + FSK
D
nucleus-enriched
cytoplasm-enriched
log2(nuclear/cytoplasmic TLK2 intensity)
control
KCl + FSK